ISSN (Print) 1226-1750
ISSN (Online) 2233-6656
Journal of Magnetics 26(4), 415-419 (2021) https://doi.org/10.4283/JMAG.2021.26.4.415

Sub-GHz Frequency Response of Anomalous Nernst Effect in the NiFe Block with Sinusoidal Laser Pulses

Seungha Yoon*

Green Energy and Nano Technology R&D Group, Korea Institute of Industrial Technology, Gwangju, South Korea

(Received 7 October 2021, Received in final form 13 December 2021, Accepted 13 December 2021)

Because the anomalous Nernst effect (ANE) involves the effective electric field generated by the combination between the thermal gradient and the magnetization direction, it has been well applied to not only the measurement of the static magnetization but also the experiment for the low frequency magnetization dynamics. In this work, the frequency response of the ANE was examined to provide two implications: First, as a method to separate Nernst effects from other signals in the homodyne or heterodyne method, and second, as a timing reference to the phase-sensitive magnetization dynamics. The intensity of 1550 nm laser power was modulated up to 2.4 GHz and successfully produced the equivalent speed of the ANE signals from the 10 nm Permalloy block on the sapphire substrate. The implications could be supported, when the detection system consists of well-designed radio frequency components and the better heat sink substrate to get the faster thermal gradient on the magnets.

Keywords : Anomalous Nernst Effect, ANE, intensity modulation

1. Introduction

Recently, the prospect of driving spin currents with the thermal gradients in spintronic devices has generated much interest in the relationships between the heat flows and the spin currents. Theoretical work has predicted that the spin currents can be driven more efficiently by the thermal gradients than by the spin filtering of electrical current passing through the ferromagnetic metals and the area of interest has earned the name "spin caloritronics". The main thermo-magnetic effects, anomalous Nernst effect (ANE) [1-9] and spin Seebeck effect [10-16], have been investigated in the various materials with the single- or multi-layers. The spin Seebeck effect is the generation of the spin current driven by the thermal gradient in the ferromagnet. This effect is analogous to the better known (non-spin) Seebeck effect used in the thermocouples. In the ferromagnet, however, the spin-up and the spin-down currents are both driven by the thermal gradient, but in the different amounts, yielding the net spin current. Such spin currents can be detected using the inverse spin Hall effect in the normal metals, where the spin orbit coupling allows the spin current to drive the transverse, detectable charged current [17-19].

The generated electric field $\vec{E}_{\mathrm{ANE}}$ between the magnetization $\vec{M}$, the thermal gradient $\vec{\nabla} T$ could be described by, in the direction perpendicular to both the magnetization and the temperature gradient.

$$\vec{E}_{\mathrm{ANE}} = -C_{\mathrm{ANE}} \mu_0 \vec{M} \times \vec{\nabla} T \tag{1}$$

In this work, the ANE toward the high-speed magnetization measurement is examined. Most studies on the spin thermoelectric effects have been focused on measuring the magnitude of its coefficient (C_{ANE}) under the dc or the low frequency of temperature gradient [20-23]. However, the frequency response of the spin thermoelectric effect at high frequency is very important for developing the spintronic devices, such as the magnetic random access memory and the magnetic sensors, in terms of the sampling rate. Recently one study has reported about 350 MHz cutoff frequency of spin Seebeck effect in YIG/Pt bilayer using the laser intensity modulations [20]. The main restriction of cutoff frequency has been understood as the combination of the low-pass behavior [24, 25] between the individual magnon modes [26-28].

*Corresponding author: Tel: +82-62-600-6580
Fax: +82-62-600-6109, e-mail: yoonsh@kitech.re.kr

2. Experimental

The anomalous Nernst effect measurements were performed on the Ti(3 nm)/Permalloy(10 nm)/Ti(3 nm) block (150 μm×500 μm, rectangle), deposited on the thick sapphire substrate using the ultra-high vacuum sputter. The 200 nm thick Au contact pads were deposited to collect the anomalous Nernst signals from the Permalloy block. Because the Ti layer exhibits very small spin Hall angles, the ANE became the dominant effect in this study rather than spin Seebeck effect. Our measurement setup and the patterned sample are shown in Fig. 1. The intensity of 1550 nm laser is modulated using the fiber based intensity modulator (IM) and focused on the Permalloy surface using the conventional plano-convex lens down to the spot size of 20 μm. The *x*-*y* stage translates the sample under the fixed laser to get the 2D images. The vector network analyzer supplies the reference signals to drive the IM and collects the amplified ANE signals between the two Au contacts in the *x*-direction. The isolated magnetization-dependent signals by taking the voltage difference between the Au pads were measured under the applied magnetic fields of 11 mT in the *y*-direction. Because of the restriction of spin Seebeck effect of the Permalloy layer, ANE could address the much wider cutoff frequency range to provide an additional reference phase signals to mix the magnetization dynamics from under the homodyne or the heterodyne detection method.

The theoretical model has considered the sinusoidal heated film surface in order to highlight the large difference between the frequency responses of the temperature (T) and the thermal gradient (dT/dz). The classical thermal diffusion equation is listed below,

$$\frac{1}{\alpha}\frac{\partial T}{\partial t} = \nabla^2 T + \frac{1}{\kappa}Q(r, t), \tag{2}$$

where α is the thermal diffusivity, κ is the thermal conductivity and Q is the heating flux due to the laser. The laser power of Gaussian beam profile and oscillating time dependence are shown as,

$$Q(r, t) = \frac{q_0}{2\pi\sigma^2} e^{-x^2/2\sigma^2} e^{-i\omega t}, \tag{3}$$

where q_0 is the net laser power, σ is the spot size, and the heat from the absorbed laser power is generated at the free surface of the sample ($z = 0$). The thorough model would requires incorporating the individual layer material properties as well as the interfacial thermal resistance, but the primary effect might be captured by the much simpler model.

3. Result and Discussion

First, the intensity of the anomalous Nernst voltages was investigated using the continuous laser power, which arose the thermal gradient at the center of the 150 μm width Permalloy sample in the *z*-axis. In the measurement scheme of the Fig. 1(a), the vector network analyzer (VNA) was replaced by a conventional digital voltmeter, therefore, the dc anomalous Nernst signals depending on the magnetization were collected. The relative anomalous Nernst voltages depending on the laser power at the center Permalloy are shown in the Fig. 2(a), when the magnetic field varied in the *y*-axis. It is clearly shown that the anomalous voltage is proportional to the incident laser power (370 mW incident power produced 10 times larger

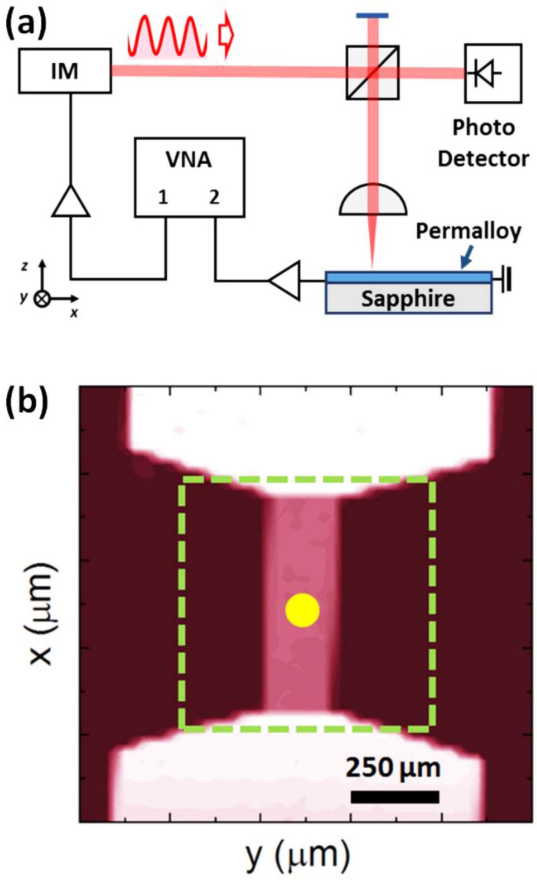

Figure 1. (Color online) (a) Schematic of the apparatus. A continuous 1550 nm wavelength laser beam is modulated by a fiber-based intensity modulator (IM), and focused on a 10 nm thick Permalloy block on a sapphire substrate. The vector network analyzer (VNA) feeds ac current to the IM and receives the amplified anomalous Nernst signals. (b) The reflection image shows the Permalloy block, 150 × 500 μm^2, and 200 nm Au contact pads on the sapphire substrate. The *x*-*y* stage moves the Permalloy sample under the fixed beam position for 2D scan.

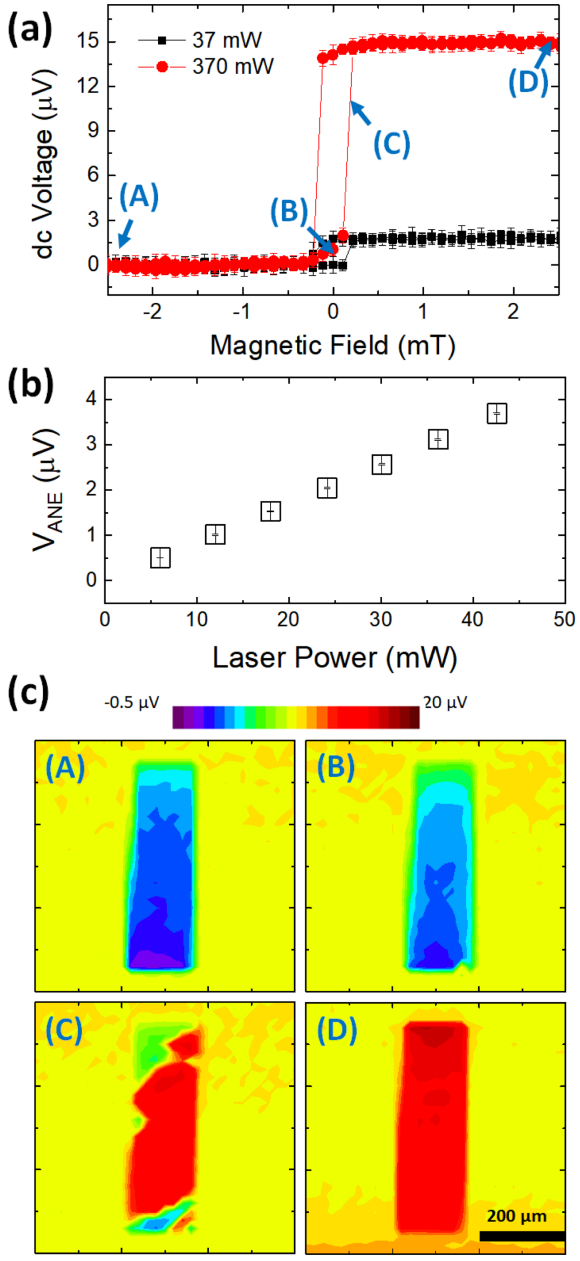

Figure 2. (Color online) (a) The magnetic hysteresis curves from the dc anomalous Nernst signals using 37 mW (black, square) and 370 mW (red, circle) laser power, where the continuous laser was focused on the center of the Permalloy block. (b) The variation of anomalous Nernst voltages depending on the laser power, where the power varied from 5 mW to 45 mW. (c) The color images indicate the y-magnetization component corresponding to the status (A), (B), (C), and (D) in the graph (a). The image area is shown in the Fig. 1(b) as the dot-green box.

signal than 37 mW). The linear relation between the ANE signal and the laser power was precisely examined in the Fig. 2(b), when the laser power varied from 5 mW to 45 mW. Because the Permalloy film thickness was quite

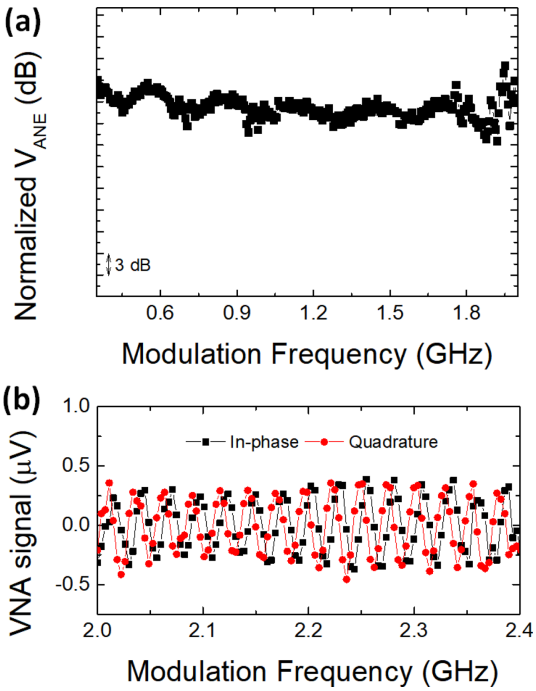

Figure 3. (Color online) (a) the normalized magnitude of anomalous Nernst signals for the modulation frequency ranges between 0.35 to 2.0 GHz. The effective path length mainly causes the oscillation period of both the in-phase and the quadrature signals and systematic error arise the lower signal oscillations. (b) The in-phase and quadrature signals of the vector network analyzer when the modulation frequency varied from 2.0 GHz to 2.4 GHz.

smaller than that of the substrate, therefore, the temperature gradient would be thought that the thermal conductivity of the sapphire drove the linear relation between the laser power and the ANE voltage. Because the anomalous Nernst coefficient $C_{ANE} \approx 1.96 \times 10^{-7}$ V $(K \cdot T)^{-1}$ of the Permalloy has been well known from the previous studies [21, 22, 29], it could be also estimated that the temperature gradient in the Permalloy 10 nm was 2 K, when the laser power was 370 mW.

Because the anomalous Nernst voltage directly shows the magnetization direction of the ferromagnet, the 2D magnetization image during the reversal process could be measured as a function of the external magnetic field. The color images in the Fig. 2(c) show the magnetic y-components (M_y) corresponding to the magnetic fields as marked as the alphabet in the Fig. 2(a) at the laser power of 370 mW. When the magnetization was parallel to the magnetic field in the y-axis, (A), (B) and (D) showed the single domain states either in the positive or the negative y-direction. During the magnetization reversal of the Permalloy block, the intermediate magnetization state (C) indicated the domain walls. It means that the intermediate

states of the micro-/nano-patterns in the magnetic sensor, the memory and the logic device could be well defined using the ANE measurement, when the spot size is sufficiently decreased under sub-micrometer using the objective lens.

Next, the dc voltmeter was replaced to the VNA to confirm the frequency response of the ANE signal, when the thermal gradient frequency increased up to sub-GHz. The sinusoidal heating effect on the Permalloy surface was induced by the intensity modulation of 22 mW laser and observed by the VNA directly, when the modulation frequency varied from 350 MHz to 2.4 GHz. As shown in the Fig. 3(a), there was no significant intensity drop of ANE magnitude during the modulation frequency sweep of laser power. The effective path including the optical path, the cable length, and the unsuitable contacts produced the large oscillation of the magnitude of ANE signal. However, unexpected noise were shown in the frequency range from 1.9 GHz to 2.0 GHz in the Fig. 3(b). Above the 2.0 GHz, the signal maintains the stable phase condition between the in-phase and the quadrature voltages, as shown in Fig. 3(b). There might be several reasons to explain this restriction. First of all, comparing to the low modulation frequency modulations (< 1 MHz), the anomalous Nernst signals are very sensitive to the laser power fluctuations at sub-GHz frequency. Second, the detection patterns are also precisely prepared to get the RF signals. Therefore, the sufficient chopping technique and the coplanar waveguide pattern will be needed to secure the ANE amplitude in the RF ranges.

4. Conclusion

The frequency response of ANE was measured in the Permalloy 10 nm block on the sapphire substrate. The fast variation of the heat flux was manipulated by the modulation of laser intensity using the electro-optical modulator up to 2.4 GHz. The frequency dependence of the in-phase, the quadrature, and the phase signals were verified by the VNA. Because of the frequency restriction of the VNA and the systematic imperfection of the coplanar waveguide design, a higher RF frequency is not determined in this study. However, 2.4 GHz is about six times higher than the cutoff frequency of the previous spin Seebeck study. Because the ANE could verify the magnetization direction of the ferromagnetic material in the specific axis. It could be widely used for measuring both the static and the dynamic magnetizations in the wide frequency ranges. In particular, the ANE's large bandwidth could provide additional reference signal in the phase sensitive homo/heterodyne experiments.

Acknowledgement

This work is supported by Korea Institute of Industrial Technology (KITECH).

References

[1] K. Uchida, T. Kikkawa, T. Seki, T. Oyake, J. Shiomi, Z. Qiu, K. Takanashi, and E. Saitoh, Phys. Rev. B **92**, 94414 (2015).
[2] S. Y. Huang, W. G. Wang, S. F. Lee, J. Kwo, and C. L. Chien, Phys. Rev. Lett. 1**07**, 216604 (2011).
[3] T. Miyasato, N. Abe, T. Fujii, A. Asamitsu, S. Onoda, Y. Onose, N. Nagaosa, and Y. Tokura, Phys. Rev. Lett. **99**, 86602 (2007).
[4] W.-L. Lee, S. Watauchi, V. L. Miller, R. J. Cava, and N. P. Ong, Phys. Rev. Lett. **93**, 226601 (2004).
[5] N. Hanasaki, K. Sano, Y. Onose, T. Ohtsuka, S. Iguchi, I. Kézsmárki, S. Miyasaka, S. Onoda, N. Nagaosa, and Y. Tokura, Phys. Rev. Lett. **100**, 106601 (2008).
[6] D. Meier, D. Reinhardt, M. Schmid, C. H. Back, J.-M. Schmalhorst, T. Kuschel, and G. Reiss, Phys. Rev. B **88**, 184425 (2013).
[7] K. Behnia and H. Aubin, Rep. Prog. Phys. **79**, 46502 (2016).
[8] C. Fang, C. H. Wan, Z. H. Yuan, L. Huang, X. Zhang, H. Wu, Q. T. Zhang, and X. F. Han, Phys. Rev. B **93**, 54420 (2016).
[9] G. Y. Guo, Q. Niu, and N. Nagaosa, Phys. Rev. B **89**, 214406 (2014).
[10] K. Uchida, S. Takahashi, K. Harii, J. Ieda, W. Koshibae, K. Ando, S. Maekawa, and E. Saitoh, Nature **455**, 778 (2008).
[11] M. Agrawal, V. I. Vasyuchka, A. A. Serga, A. Kirihara, P. Pirro, T. Langner, M. B. Jungfleisch, A. V. Chumak, E. T. Papaioannou, and B. Hillebrands, Phys. Rev. B **89**, 224414 (2014).
[12] C. M. Jaworski, J. Yang, S. Mack, D. D. Awschalom, R. C. Myers, and J. P. Heremans, Phys. Rev. Lett. **106**, 186601 (2011).
[13] C. M. Jaworski, J. Yang, S. Mack, D. D. Awschalom, J. P. Heremans, and R. C. Myers, Nat. Mater. **9**, 898 (2010).
[14] K. Uchida, H. Adachi, T. Ota, H. Nakayama, S. Maekawa, and E. Saitoh, Appl. Phys. Lett. **97**, 172505 (2010).
[15] K. Uchida, H. Adachi, T. An, T. Ota, M. Toda, B. Hillebrands, S. Maekawa, and E. Saitoh, Nat. Mater. **10**, 737 (2011).
[16] M. Schreier, A. Kamra, M. Weiler, J. Xiao, G. E. W. Bauer, R. Gross, and S. T. B. Goennenwein, Phys. Rev. B **88**, 94410 (2013).
[17] O. Mosendz, V. Vlaminck, J. E. Pearson, F. Y. Fradin, G. E. W. Bauer, S. D. Bader, and A. Hoffmann, Phys. Rev. B **82**, 214403 (2010).
[18] L. Liu, C.-F. Pai, Y. Li, H. W. Tseng, D. C. Ralph, and R.

A. Buhrman, Science **336**, 555 (2012).
[19] B. F. Miao, S. Y. Huang, D. Qu, and C. L. Chien, Phys. Rev. Lett. **111**, 66602 (2013).
[20] M. Schreier, F. Kramer, H. Huebl, S. Geprägs, R. Gross, S. T. B. Goennenwein, T. Noack, T. Langner, A. A. Serga, B. Hillebrands, and V. I. Vasyuchka, Phys. Rev. B **93**, 224430 (2016).
[21] M. Weiler, M. Althammer, F. D. Czeschka, H. Huebl, M. S. Wagner, M. Opel, I.-M. Imort, G. Reiss, A. Thomas, R. Gross, and S. T. B. Goennenwein, Phys. Rev. Lett. **108**, 106602 (2012).
[22] M. Schmid, S. Srichandan, D. Meier, T. Kuschel, J.-M. Schmalhorst, M. Vogel, G. Reiss, C. Strunk, and C. H. Back, Phys. Rev. Lett. **111**, 187201 (2013).
[23] K.-D. Lee, D.-J. Kim, H. Yeon Lee, S.-H. Kim, J.-H. Lee, K.-M. Lee, J.-R. Jeong, K.-S. Lee, H.-S. Song, J.-W. Sohn, S.-C. Shin, and B.-G. Park, Sci. Rep. **5**, 10249 (2015).
[24] N. Roschewsky, M. Schreier, A. Kamra, F. Schade, K. Ganzhorn, S. Meyer, H. Huebl, S. Geprägs, R. Gross, and S. T. B. Goennenwein, Appl. Phys. Lett. **104**, 202410 (2014).
[25] A. Brataas, Y. V. Nazarov, and G. E. W. Bauer, Phys. Rev. Lett. **84**, 2481 (2000).
[26] S. M. Rezende, R. L. Rodríguez-Suárez, J. C. Lopez Ortiz, and A. Azevedo, Phys. Rev. B 89, 134406 (2014).
[27] E. G. Spencer and R. C. LeCraw, Proc. IEE - Part B Electron. Commun. Eng. **109**, 66 (1962).
[28] A. D. Avery, S. J. Mason, D. Bassett, D. Wesenberg, and B. L. Zink, Phys. Rev. B **92**, (2015).
[29] T. Kikkawa, K. Uchida, S. Daimon, Y. Shiomi, H. Adachi, Z. Qiu, D. Hou, X.-F. Jin, S. Maekawa, and E. Saitoh, Phys. Rev. B **88**, 214403 (2013).